Communications in Physics, Vol. 34, No. 1 (2024), pp. 45-56
DOI: https://doi.org/10.15625/0868-3166/18878

Effect of precursor and calcination time on the morphological structure and catalytic activity of Co_3O_4 film in the oxygen evolution reaction

Nguyen Thi Giang[1], **Pham Hong Hanh**[1], **Ngo Thi Anh Tuyet**[1], **Vu Thi Kim Oanh**[2,3], **Do Chi Linh**[1], **Nguyen Duc Lam**[1], **Nguyen Thi Mai**[1], **Hoa Thi Bui**[1,†] **and Nguyen Thanh Tung**[1,2,‡]

[1]*Institute of Materials Science, Vietnam Academy of Science and Technology, Hanoi 100000, Vietnam*

[2]*Graduate University of Science and Technology, Vietnam Academy of Science and Technology, Hanoi 100000, Vietnam*

[3]*Institute of Physics, Vietnam Academy of Science and Technology, Hanoi 100000, Vietnam*

E-mail: [†]hoabt@ims.vast.ac.vn; [‡]tungnt@ims.vast.ac.vn

Received 11 September 2023
Accepted for publication 10 January 2024
Published 5 February 2024

Abstract. *This research investigates the effect of cobalt precursor and calcination time on the morphology and catalytic activity of Co_3O_4 films in the oxygen evolution reaction (OER). Co_3O_4 films with porous flower-like nanostructures were obtained using cobalt nitrate as a cobalt precursor, while cobalt chlorides were used to produce porous nanoneedle structures Co_3O_4 film. Extended annealing time at temperature 350˚C caused structural fractures in the films. Among the samples, the synthesized Co_3O_4 films were then evaluated as catalyst materials for the OER in alkaline 1M KOH electrolyte. Among synthesized films, the Co_3O_4-2-1h, synthesized using the cobalt chlorides as Co precursor and annealed at 350˚C for 1 hour, exhibited better OER catalytic activity. With its porous nanoneedle structure, the Co_3O_4-2-1h demonstrated superior performance comparable to the state-of-the-art 20% Ir/C catalyst. Moreover, the Co_3O_4-2-1h film demonstrated remarkable stability for the OER in a 1M KOH alkaline electrolyte.*

Keywords: Co_3O_4; film; precursor; calcination time; OER.

Classification numbers: 79.60.Jv; 87.23.-n; 88.20.fn.

1. Introduction

Fossil fuels (coal, petroleum, natural gas,....) continue to be the primary source of energy, supplying more than 80% of energy demand of the world. However, the use, extraction, and combustion of these fossil fuels have caused significant environmental issues such as air pollution, acid rain, climate change, directly impacting human life and health [1, 2]. Therefore, research and development of new, low-cost, clean, and sustainable energy to replace fossil fuels have become crucial [3, 4]. Among alternative energy, hydrogen is considered as one of the most potential energy supplies in future due to its high density energy. Additionally, hydrogen is carbon-free, so the combustion product is only water (H_2O), which does not emit harmful gases to the environment and humans. However, hydrogen does not exist naturally, and water splitting is currently considered the best technology for hydrogen production through electrochemical energy [5, 6]. Water splitting is the simultaneous combination of two half-reactions: the oxygen evolution reaction (OER) at the anode and the hydrogen evolution reaction (HER) at the cathode. While the HER requires 2 electrons to release one H_2 molecule, the OER with a four-electron transfer process at the anode to generate one O_2 molecule ($2H_2O \longrightarrow O_2 + 4H^+ + 4e^-$), which is the bottleneck for water splitting, is a challenging with slow kinetics and low energy conversion efficiency [7, 8]. The catalyst plays a important role in the OER, accelerating reaction rate and improving electrocatalytic efficiency. Up to now, IrO2 and RuO2 have been the most effective catalysts for the OER, but their cost and availability pose disadvantages when applied on an industrial scale [9, 10]. Therefore, the research and development of alternative catalyst materials with high catalytic activity, good efficiency, and low cost for the OER are being highly emphasized. First-row transition metals such as Co, Ni, Fe, Mn ... have attracted much attention due to their tunable chemical reactivity based on crystal structure and electronic properties, theoretical high efficiency, thermodynamic stability, and corrosion resistance [11]. Among them, Co_3O_4 with a spinel structure has shown promising electrocatalytic activity and outstanding chemical stability in alkaline environments [12–14]. However, similar to most materials, the OER catalytic activity of Co_3O_4 depends on synthesis conditions as precursors, and sample treatment temperatures. Co_3O_4 can be easily synthesized as powder with particle structures, then used to create inks with a supporting material, and subsequently deposited on the electrode surface [15]. However, this method is time-consuming for preparation and adversely affects the electrochemical activity, OER catalytic durability, and overall electrochemical properties due to the use of supporting materials and additional processes like grinding and milling that increase contact resistance and alter particle size [16]. Therefore, the research and fabrication of Co_3O_4 film directly on the electrode substrate are highly necessary as using the substrate directly as the electrode will not affect the intrinsic activity and durability of the OER catalyst. Furthermore, recent studies have shown that the OER activity of catalysts depends greatly on the number of active catalytic sites and the contact of these active sites with the electrolyte [16, 17].

Hence, this research report investigates the effect of synthesis conditions: precursor and calcination time on morphological structure and catalytic activity of Co_3O_4 film in the OER in alkaline electrolyte. The use of Cobalt nitrate as precursor results in the synthesis of Co_3O_4 films with a porous flower-like nanostructure, while the cobalt chlorides precursor yields porous nanoneedle Co_3O_4 films. Furthermore, annealing at temperatures above 350°C for 2 hours or more leads to

structural fractures. The synthesized Co_3O_4 films were investigated for their application as catalyst materials in the OER in 1M KOH alkaline medium. Among them, the Co_3O_4-2-1h sample, synthesized using the Cl- precursor and annealed at 350˚C for 1 hour, exhibited the advanced OER catalytic activity. The Co_3O_4-2-1h sample displayed a porous nano-needle structure and demonstrated superior performance that could compete with state of the art 20% Ir /C. Furthermore, the Co_3O_4-2-1h film also performed stability against OER in the 1M KOH alkaline electrolyte.

2. Experiment

2.1. Materials

The chemicals $Co(NO_3)2.6H_2O$, $CoCl_2.6H_2O$, Urea (NH_2CONH_2), and KOH from Sigma Aldrich were used as received. Deionized water (DI H_2O) served as the solvent. Carbon fiber paper (CFP) was used as the substrate for electrochemical measurements, while Fluorine-doped Tin Oxide (FTO) glass was used for XRD characterization. Before using, the substrate was cleaned by ultrasonication in DI water, acetone, and ethanol solution for 15 minutes each, followed by air-drying at room temperature.

2.2. Preparation of Co_3O_4-1-1h, Co_3O_4-1-2h, Co_3O_4-2-1h and Co_3O_4-2-2h

To prepare Co_3O_4 films on substrates, two different precursors, $Co(NO_3)_2$ $.6H_2O$ and $CoCl_2.6H_2O$, were used in a two-step synthesis process involving hydrothermal and subsequent thermal treatment.

When using $Co(NO_3)_2.6H_2O$ as the precursor, a Cobalt hydroxycarbonate (Co-HC-1) film was synthesized by mixing 0.1M $Co(NO_3)_2.6H_2O$ and 0.3M Urea and subjecting the mixture to synthesis at 90˚C for 5 hours. The resulting Co-HC-1 film was then washed, dried, and stored at room temperature. In the second step, the Co-HC-1 film was heated at 350˚C for different calcination times of 1 hour and 2 hours to form Co_3O_4-1-1h and Co_3O_4-1-2h films, respectively.

Similarly, to the above procedure, using $CoCl_2.6H_2O$ as the precursor, the Co-HC-2 film was prepared by heating a mixture of 0.1M $CoCl_2.6H_2O$ and 0.3M Urea at 90˚C for 5 hours. Subsequently, the Co-HC-2 film is calcinated at 350˚C for different calcination times of 1 hour and 2 hours to form Co_3O_4-2-1h and Co_3O_4-2-2h films, respectively. The resulting films were then stored for further experiments.

2.3. Film characterizations

The crystal structure of synthesized films was determined using an X-ray diffraction instrument (Rigaku D/MAX 2600 V) with Cu K_α radiation (λ = 0.15418 nm) at a scanning rate of 3˚/minute. The surface morphology of the films was examined using a Field Emission Scanning Electron Microscope (FE-SEM, HITACHI S-4800) at an accelerating voltage of 15 kV. Moreover, the sample is analyzed using a high-resolution transmission electron microscope (HR-TEM, Jeol) operating at 200 kV.

2.4. Electrochemical measurement

The electrochemical measurement was conducted using a three-electrode system, including a Pt-wire as the counter electrode, an Ag/AgCl (3 M KCl) as the reference electrode, and the films were deposited on a CFP substrate as the working electrode. A potentiostat (Metrohm – Autolab) was used for the measurements. The electrocatalytic performance of the synthesised

films on OER was evaluated using linear sweep voltammetry in an alkaline electrolyte (1.0 M KOH) with a sweeping rate of 10 mVs^{-1}. The potential range was from 1.10 to 2 V vs RHE (Reversible Hydrogen Electrode). To convert the bias potential ($E_{Ag/AgCl}$) applied against the Ag/AgCl reference electrode into the potential on the RHE scale as follow equation: E (RHE) = $E_{Ag/AgCl}$ + 0.059pH + $E^0{}_{Ag/AgCl}$, where $E^0{}_{Ag/AgCl}$= 0.21 V at 25 ˚C [18]. Furthermore, to study the stability of synthesized film in the OER activity, cyclic voltammetry (CV) was measured in 1000 cycles within the potential range of 1.2-1.65 V vs RHE.

3. Results and discussions

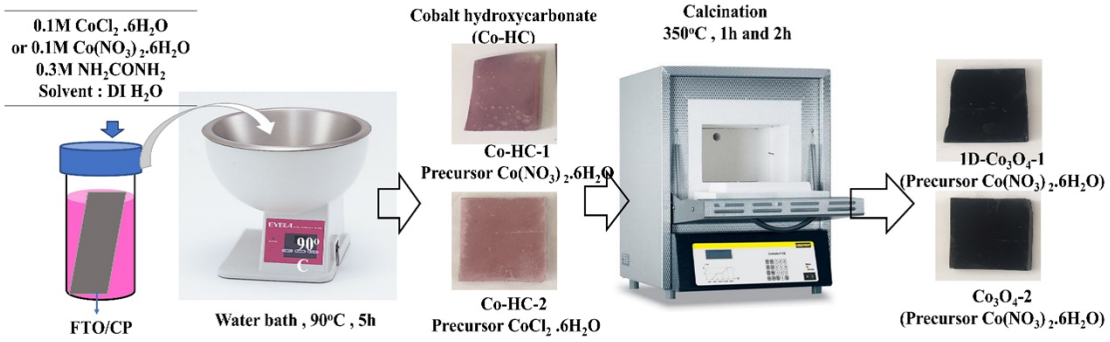

Scheme 1. Synthesis process of Co_3O_4 using different Co precursors, in which Co_3O_4-1 film is produced using cobalt nitrate as the Co precursor, and Co_3O_4-2 film is produced using cobalt chlorides as the Co precursor.

Scheme 1 illustrates the synthesis process of Co_3O_4 using different Co precursors, in which Co_3O_4-1 film is produced using cobalt nitrate as the Co precursor, and Co_3O_4-2 film is produced using cobalt chlorides as the Co precursor. In the first step, a cobalt hydroxycarbonate film is prepared on the surface of the substrate (carbon paper and FTO glass) through a hydrothermal method, following the subsequent (1) (2), (3) reactions. Subsequently, the cobalt hydroxycarbonate film is annealed at a temperature of 350˚C for 1 hour and 2 to obtain oxides films.

$NH_2CONH_2 + 3H_2O \longrightarrow 2NH_4^+ + 2OH^- + CO_2$ (reaction 1)

$CO_2 + 2OH^- \longrightarrow CO_3^{2-} + H_2O$ (reaction2)

$Co^{2+} + xOH^- + 0{,}5CO_3^{2-} + 0{,}11H_2O \longrightarrow Co\ (OH)\ x\ (CO_3)_{0,5}\ 0{,}11H_2O$ (reaction3)

In scheme 1, the real images of the cobalt hydroxycarbonate films (Co-HC) film clearly show that there is a slight difference in color when different precursors are used . With the cobalt nitrate precursor, the color is darker and tends towards purple, while with the cobalt chlorides precursor, the color of the HC film tends towards pink.

The surface morphology of the synthesized films was studied by SEM. Fig. 1 (a), (b), and (c), respectively show the SEM images of the Co-HC-1, Co_3O_4-1-1h, and Co_3O_4-1-2h films, which use Cobalt nitrate as Co precursor. The images reveal that the synthesized CoHC-1 film exhibits a flower-like nanostructure. After undergoing annealing at 350˚C for 1 hour, the nanoflower structure of the Co_3O_4-1-1h sample exhibited an increase in size and developed a porous nature. However, when the Co_3O_4-1-2h film was annealed at 350˚C for 2 hours, the flower-like nanostructure started to melt as shown in Fig. 1(c). Remaining the structure after annealing

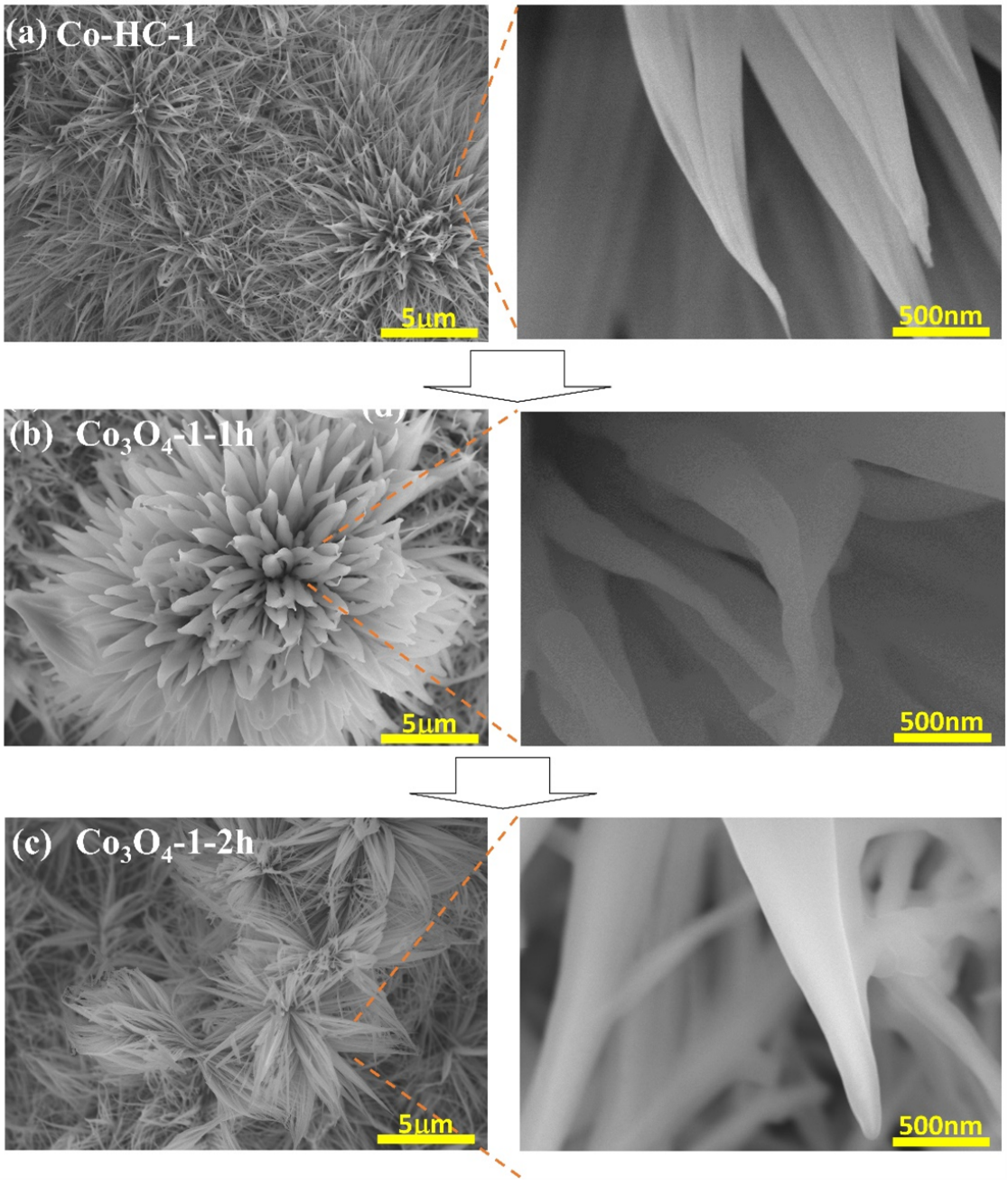

Fig. 1. SEM images of (a) CoHC-1, (b) Co_3O_4-1-1h and (c) Co_3O_4-1-2h.

for 1 hour while porous caused increases the surface area, which positively affects its physical, chemical, and electrochemical properties.

On the other hand, Figs. 2 (a), (b), and (c), respectively show the SEM images of the Co-HC-2, Co_3O_4-2-1h, and Co_3O_4-2-2h films, using Cobalt chloride as the Co precursor. From the SEM images, it can be observed that the synthesized CoHC-2 presents a nanoneedle structure. Then being thermal treatment at 350˚C for 1 hour, the Co_3O_4-2-1h sample maintains its nanoneedle structure but became porous. In the Co_3O_4-2-2h sample, when annealed at the same temperature for 2 hours, the porous nanoneedle start to break, resulting in shorter nanorods compared to the initial length. Similar to the films synthesized using cobalt nitrate as the Co precursor, annealed for 1 hour the Co_3O_4-2-1h maintains their structure while becoming porous, leading to an increased surface area. This, in turn, enhances electron mobility and activates more catalytic sites, thereby positively influencing the catalytic activity of the synthesized films.

The distinct differences in the formation of synthesized film structure and morphology when using two different salts as precursors can be explained based on the Hard-Soft Acid-Base (HSAB) principle [19]. According to this, hard acids prefer to bond with hard bases, and vice versa. Based on this concept, metal ions and ligands can be classified as hard or soft. Therefore, depending on their relative hardness, metal ions and ligands control their interactions, thus influencing the nanostructure shape of the hydroxycarbonate film. To investigate the influence of different reacting anions on the morphology, two different Co precursors: $Co(NO_3)_2$ and $CoCl_2$ were used. In the absence of any surface-active agents or complexing agents used in the present case to control the morphology, the synthetic method involved the reaction of Co ions with hydroxide ions released in situ by urea hydrolysis, as shown in reactions (1)-(3). It should be noted that the different affinities of the counter anions to the Co ions in the precursor control the local concentration of available Co ions for reaction (3), thus controlling the reaction kinetics. Therefore, the controlled release of OH^- and CO_3^{2-} ions through the slow urea hydrolysis and their reactions with different cobalt precursors can result in the controlled kinetics of reaction (3) and, consequently, different morphologies of the hydroxycarbonate film as shown in Fig. 1 and Fig. 2. In the present case, Co^{2+} acts as a weak acid and prefers to bond with a softer base more strongly than a harder base. The softness of the ligands used in these experiments follows the decreasing order of $NO_3 > Cl$. This implies that Cl forms stronger bonds with Co ions, resulting in fewer Co ions available for the controlled synthesis of the nanostructured material. In this way, the interaction between Co ions and the reacting ions plays a role in controlling the concentration of available ions for the reaction, thus controlling the shape of the product from reaction (3). These mentioned factors are considered capable of overall control over the morphology of the film. Consequently, as evident from the SEM images in Fig. 1 and Fig. 2, a nanoneedle structure is formed when using the cobalt chlorides as Co precursor, while a flower-like nano structure is obtained when using the cobalt nitrate for Co precursor.

The XRD patterns of Co-HC-1, Co-HC-2, Co_3O_4-1-1h, Co_3O_4-2-1h, Co_3O_4-2-1h, and Co_3O_4-2-2h films are displayed in Fig. 3 (a) and (b). In Fig. 3(a), the XRD patterns of Co-HC-1, Co-HC-2 films with two different salt precursors perfectly matched the XRD patterns of cobalt hydroxycarbonate ($Co(OH)_x(CO_3)_{0.5}$•$0.11H_2O$) (JCPDF #38-547). After annealing the HC films at 350˚C for 1-hour to form Co_3O_4-1-1h, Co_3O_4-2-1h, significant changes were observed in the XRD patterns, corresponding to the (111), (220), (311), (222), (400), (422), and (511) crystal planes of Co_3O_4 with JCPDF #42-1467 (Fig. 3(b)). In the Co_3O_4-1-1h and Co_3O_4-2-1h films, the peaks corresponding to the hydroxycarbonate film remain, indicating incomplete oxide formation. However, with an increased calcination time of 2 hours to form Co_3O_4-1-2h and Co_3O_4-2-2h

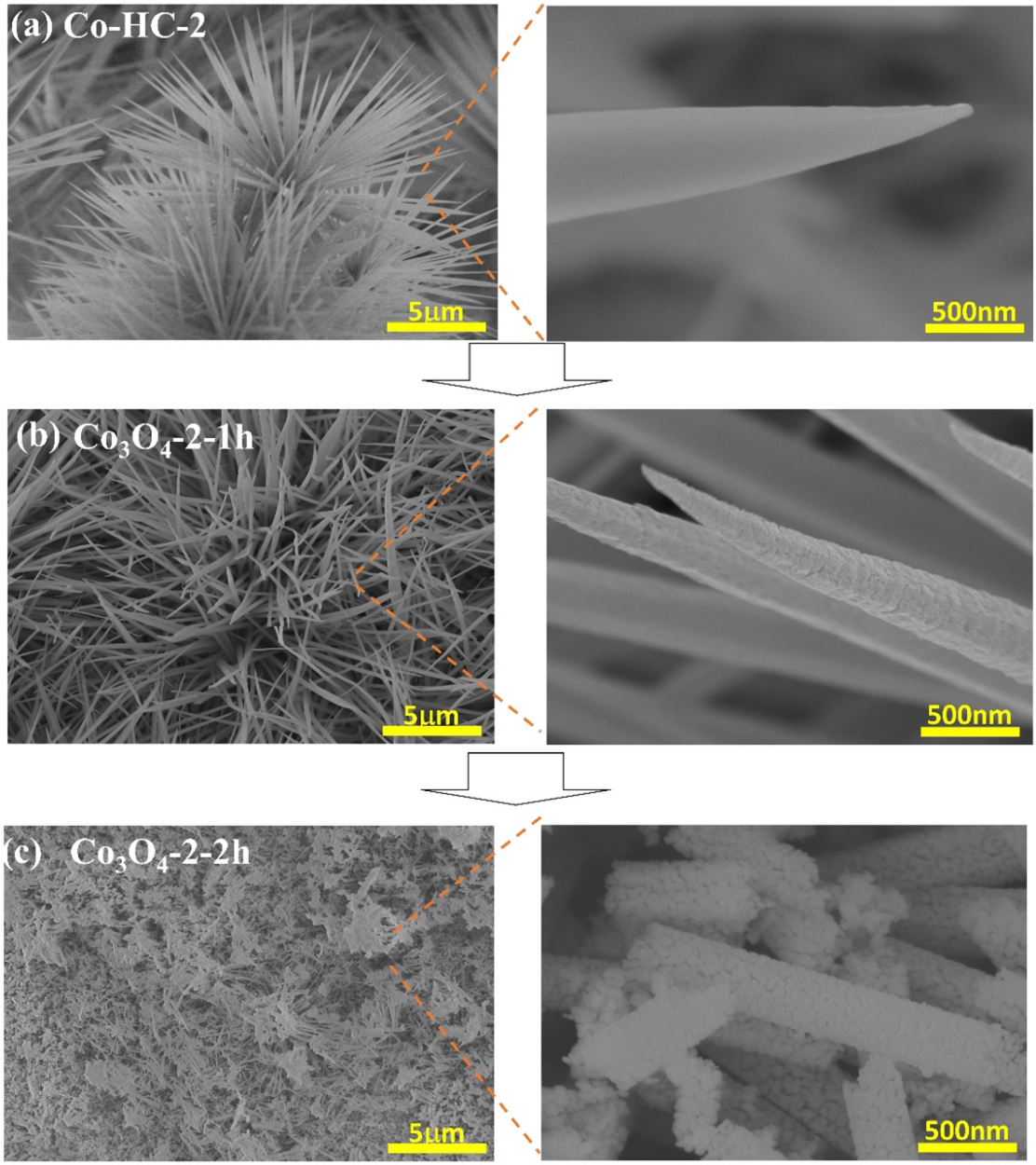

Fig. 2. SEM images of (a) CoHC-2, (b) Co_3O_4-2-1h and (c) Co_3O_4-2-2h.

films, all peaks match with Co_3O_4, and the hydroxycarbonate peaks disappear, indicating successful oxide formation with nanoneedle and flower-like nanostructured structures using two different precursors.

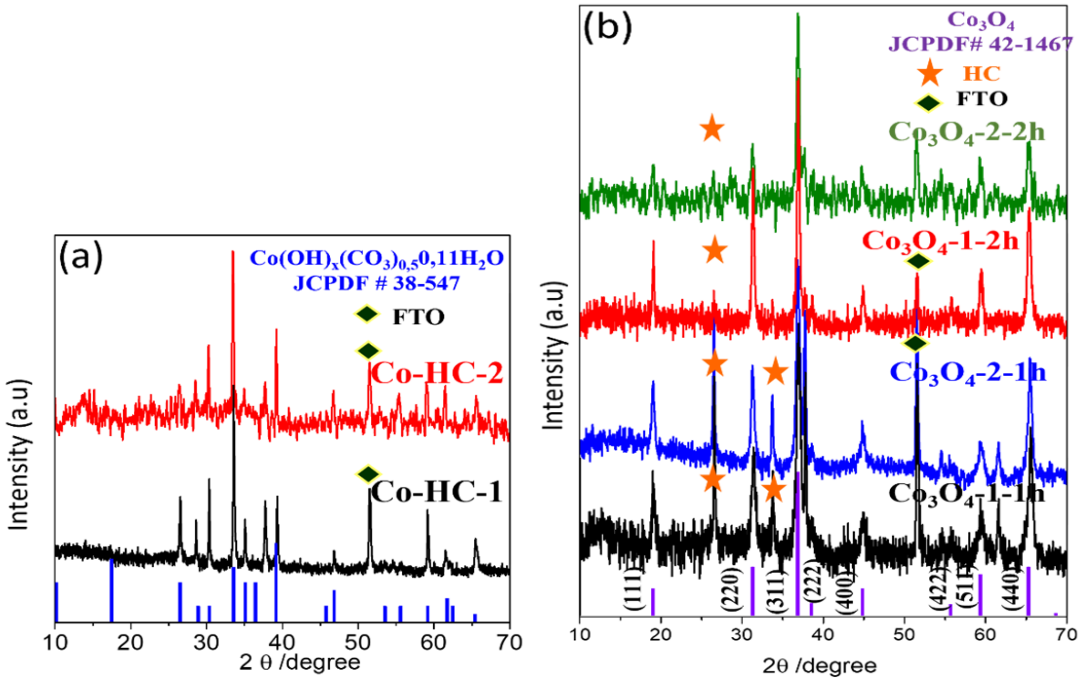

Fig. 3. XRD patterns of (a) Co-HC-1, Co-HC-2, and (b) Co_3O_4-1-1h, Co_3O_4-2-1h, Co_3O_4-2-1h, and Co_3O_4-2-2h.

To further investigate the detailed structure and crystal structure of Co_3O_4-1-1h and Co_3O_4-2-1h is studied by TEM, and the TEM, HR TEM images of Co_3O_4-1-1h and 1D-Co_3O_4-2-1h are shown in Fig. 4. Both Fig. 4(a) and (b) reveal a porous structure after annealing, with a d-spacing of 4.66 Å corresponding to the (111) plane d-spacing of Co_3O_4 (XRD patterns in Fig. 3(b)). However, a noticeable difference can be observed, wherein Fig. 4(a), the Co_3O_4-1-1h film exhibits flower-like nanostructured with larger widths compared to the nanorods in the Co_3O_4-2-1h film (in Fig. 4 (b)).

The results from SEM, XRD, and TEM demonstrate the successful synthesis of Co_3O_4 films. However, using the precursor cobalt nitrate resulted in the formation of flower-like nanostructured Co_3O_4, while the cobalt chlorides as precursor led to the synthesis of nanoneedle Co_3O_4 structures.

The Co_3O_4-1-1h, Co_3O_4-2-1h, Co_3O_4-1-2h and Co_3O_4-2-2h films on CFP used as working electrode, and their activity is investigated in OER in 1 M KOH solution. The following reactions will occur sequentially for the OER in an alkaline environment:

$M–OH_2 + OH^- \longrightarrow M–OH + H_2O + e^-$

$M–OH + OH^- \longrightarrow M–O^* + H_2O + e^-$

$M–O^* + OH^- \longrightarrow M–OOH + e^-$

$M–OOH + OH^- \longrightarrow M–OH_2 + O_2 + e^-$,

where M represents an active site on the surface of synthesized film. The species O*, OH^-, and OOH are intermediate substances that are adsorbed onto these active sites. Synthesized Co_3O_4

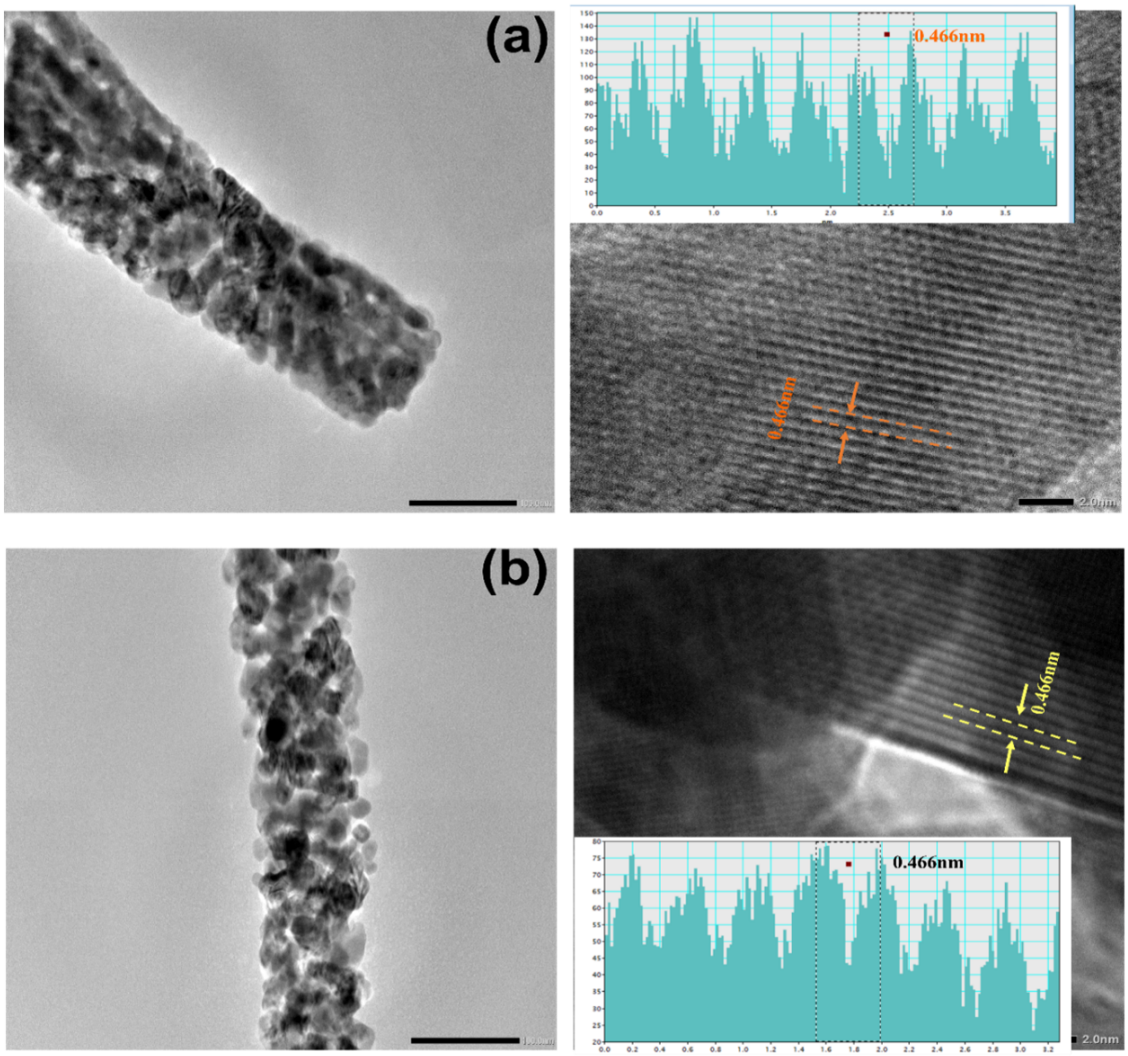

Fig. 4. TEM and HR-TEM images of (a) Co_3O_4-1-1h and (b) 1D-Co_3O_4-2-1h.

films provides active sites on its surface where the OER takes place. These active sites can undergo a series of redox reactions involving the transfer of electrons and oxygen atoms. Fig. 5 (a) shows the LSV curves of Co_3O_4-1-1h, Co_3O_4-2-1h, Co_3O_4-1-2h, Co_3O_4-2-2h and Ir (20%C) in OER in a alkaline medium (1M KOH). Co_3O_4-1-1h and Co_3O_4-2-1h films exhibit better activity than Co_3O_4-1-2h and Co_3O_4-2-2h films. The Co_3O_4-1-2h and Co_3O_4-2-2h films, when annealed for 2 hours, exhibit gradually broken structures (Fig. 1(c) and Fig. 2(c)), resulting in shorter and more complex electron transport paths, leading to reduced catalytic activity. On the other hand, annealing for 1 hour, the Co_3O_4-1-1h and Co_3O_4-2-1h films remain flower like nanostructures and nanoneedle structure but became porous Co_3O_4, significantly increasing the surface area, while still maintaining their shape after annealing, resulting in more convenient electron transport paths.

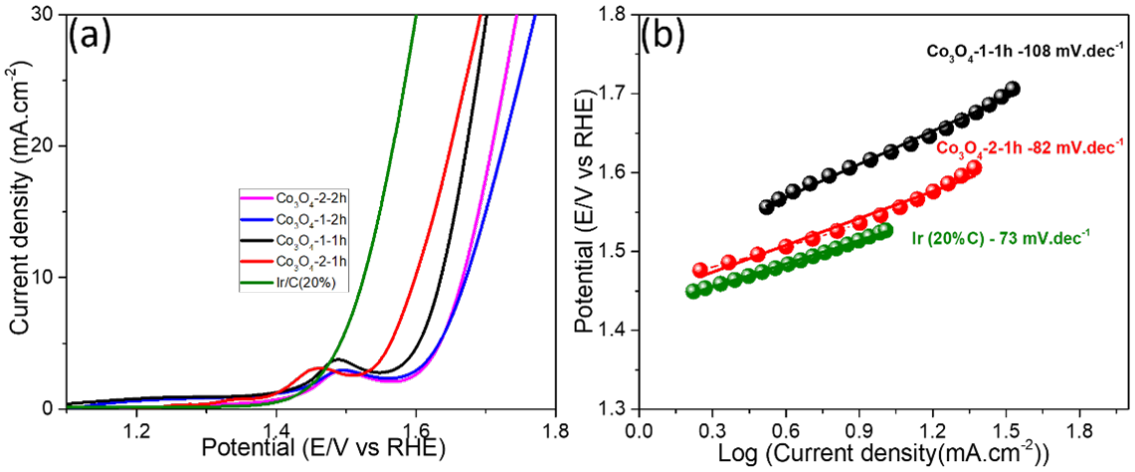

Fig. 5. (a) LSV curves of Co_3O_4-1-1h, Co_3O_4-2-1h, Co_3O_4-1-2h, Co_3O_4-2-2h, and Ir/C(20%) in OER in 1 M KOH electrolyte, and (b) their corresponding Tafel slopes.

Therefore, the Co_3O_4-1-1h and Co_3O_4-2-1h films, which were annealed for 1 hour, demonstrate significantly enhanced catalytic activity in comparison to the Co_3O_4-1-2h and Co_3O_4-2-2h films annealed for 2 hours. Among the two samples annealed for 1 hour, Co_3O_4-2-1h with a straight nanoneedle structure demonstrates better OER catalytic activity than Co_3O_4-1-1h with a flower like nanostructure. This is attributed to the structural differences between the nanoneedle structure and flower like nanostructure, where the straight nanoneedle structure leads to shorter electron transport paths and maximizes the surface area utilization in the electrolyte [20, 21]. Additionally, in the potential range of 1.4-1.6Vvs RHE, the formation of a peak is observed, which is attributed to oxidation/reduction process in the Co_3O_4 films. This process involves the interconversion between Co(II), Co(III), and Co(IV) oxidation states within the dimeric Co redox centers: $Co^{II}Co^{III} \leftrightarrow Co^{III}Co^{III} \leftrightarrow Co^{IV}Co^{III} \leftrightarrow Co^{IV}Co^{IV}$ [22–25]. Additionally, to compare the OER catalytic activity, a commercial Ir/C (20%) catalyst electrode was studied. Fig. 5 (a) demonstrates that the OER catalytic activity of Co_3O_4-2-1h is relatively good and can compete with Ir/C (20%). The Tafel slope is an intrinsic parameter for evaluating the OER kinetics of a catalyst material, and Fig. 5(b) represents the corresponding Tafel slopes of Co_3O_4-1-1h, Co_3O_4-2-1h, and Ir/C (20%). It can be observed that the Tafel slopes of Co_3O_4-1-1h, Co_3O_4-2-1h films, and Ir(20%C) are 108, 82, and 73 $mV.dec^{-1}$, respectively. These results indicate that the Tafel slope of Co_3O_4-2-1h is close to that of Ir/C (20%). Based on the catalytic activity, among all the synthesized Co_3O_4 films, Co_3O_4-2-1h with a porous nanoneedle structure exhibits the advanced OER catalytic activity.

Furthermore, the CV curves of 1000 cycles are performed to test the electrochemical stability of the synthesized Co_3O_4-2-1h films. Fig. 6 represents the CV curves Co_3O_4-2-1h in OER in the range of 1.2V-1.65V vs RHE with 1000 cycles at a scan rate of 50 $mV.s^{-1}$. The results show that after 1000 cycles of CV, the Co_3O_4-2-1h film exhibits almost no decrease or change in the shape of the CV compared to the 1st CV. This indicates that Co_3O_4-2-1h film is highly stable for OER in alkaline 1M KOH electrolyte.

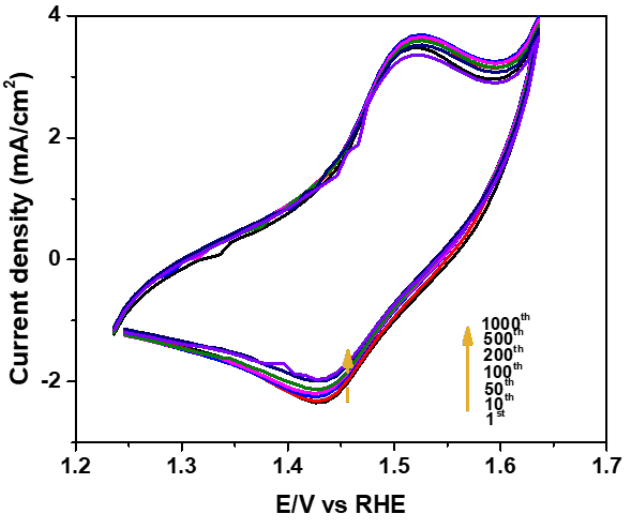

Fig. 6. CV curves of Co_3O_4-2-1h in OER in the range of 1.2V-1.65V vs RHE with 1000 cycles.

4. Conclusions

In summary, this study investigated the impact of precursor and calcination time on the morphology and OER catalytic activity of Co_3O_4 films. Using cobalt nitrate resulted in porous flower-like nanostructures, while cobalt chlorides led to porous nanoneedle structures. Extended annealing time resulted in the formation of structural fractures. Among the samples, the Co_3O_4-2-1h film synthesized with the cobalt chlorides as Co precursor and annealed for 1 hour at 350˚C demonstrated excellent OER catalytic activity, comparable to the state-of-the-art 20% Ir/C catalyst. In addition, the Co_3O_4-2-1h film exhibited stability against OER in the 1M KOH alkaline electrolyte. These findings emphasize the importance of synthesis conditions in tailoring Co_3O_4 film properties for efficient OER applications in alkaline environments.

Acknowledgment

This work is supported by Vietnam Academy of Science and Technology under grant number TĐHYD0.04/22-24.

References

[1] C. Tryggestad, N. Sharma, O. Rolser, B. Smeets, M. Wilthaner, J. van de Staaij *et al.*, *Global Energy Perspective 2022: Executive Summary*, McKinsey & Company: New York, NY, USA (2022) 26.

[2] K. Kwiatkowski, V. Singer and S. Smit, *Economic conditions outlook, June 2022*, McKinsey & Company: New York, NY, USA (2022) 28.

[3] K. Alanne, S. Cao, *An overview of the concept and technology of ubiquitous energy*, Appl. Energy. **238** (2019) 284.

[4] J. Incer-Valverde, A. Korayem, G. Tsatsaronis and T. Morosuk, *"Colors" of hydrogen: Definitions and carbon intensity*, Energy Convers. Manag. **291** (2023) 117294.

[5] D. Chen, C.-L. Dong, Y. Zou, D. Su, Y.-C. Huang, L. Tao *et al.*, *In situ evolution of highly dispersed amorphous CoOx clusters for oxygen evolution reaction*, Nanoscale **9** (2017) 11969.

[6] S. Wang, A. Lu and C.-J. Zhong, *Hydrogen production from water electrolysis: role of catalysts*, Nano Converg. **8** (2021) 4.
[7] P. Lettenmeier, J. Majchel, L. Wang, V.A. Saveleva, S. Zafeiratos, E. R. Savinova *et al.*, *Highly active nano-sized iridium catalysts: synthesis and operando spectroscopy in a proton exchange membrane electrolyzer*, Chem. Sci. **9** (2018) 3570.
[8] M. Tahir, L. Pan, F. Idrees, X. Zhang, L. Wang, J.-J. Zou, Z.L. Wang, *Electrocatalytic oxygen evolution reaction for energy conversion and storage: A comprehensive review*, Nano Energy. **37** (2017) 136.
[9] Z. Chen, X. Duan, W. Wei, S. Wang and B.-J. Ni, *Electrocatalysts for acidic oxygen evolution reaction: Achievements and perspectives*, Nano Energy **78** (2020) 105392.
[10] Q. Pan and L. Wang, *Recent perspectives on the structure and oxygen evolution activity for non-noble metal-based catalysts*, J. Power Sources. **485** (2021) 229335.
[11] X. Qin, D. Kim and Y. Piao, *Metal-organic frameworks-derived novel nanostructured electrocatalysts for oxygen evolution reaction*, Carbon Energy. **3** (2021) 66.
[12] X. Li, X. Hao, A. Abudula and G. Guan, *Nanostructured catalysts for electrochemical water splitting: Current state and prospects*, J. Mater. Chem. A. **4** (2016) 11973.
[13] N. H. Chou, P. N. Ross, A. T. Bell and T. D. Tilley, *Comparison of Cobalt-based Nanoparticles as Electrocatalysts for Water Oxidation*, ChemSusChem. **4** (2011) 1566.
[14] M. Zhang, M. de Respinis, H. Frei, *Time-resolved observations of water oxidation intermediates on a cobalt oxide nanoparticle catalyst*, Nat. Chem. **6** (2014) 362.
[15] C. Yuan, H. Bin Wu, Y. Xie and X. W. (David) Lou, *Mixed Transition-Metal Oxides: Design, Synthesis, and Energy-Related Applications*, Angew. Chemie Int. Ed. **53** (2014) 1488.
[16] S. Y. Shajaripour Jaberi, A. Ghaffarinejad, Z. Khajehsaeidi, *The effect of annealing temperature, reaction time, and cobalt precursor on the structural properties and catalytic performance of CoS2 for hydrogen evolution reaction*, Int. J. Hydrogen Energy. **46** (2021) 3922.
[17] S. A. Patil, D. V. Shinde, I. Lim, K. Cho, S.S. Bhande, R.S. Mane, *et al.*, *An ion exchange mediated shape-preserving strategy for constructing 1-D arrays of porous $CoS_{1.0365}$ nanorods for electrocatalytic reduction of triiodide*, J. Mater. Chem. A. **3** (2015) 7900.
[18] H. T. Bui, N. K. Shrestha, S. Khadtare, C. D. Bathula, L. Giebeler *et al.*, *Anodically grown binder-free nickel hexacyanoferrate film: toward efficient water reduction and hexacyanoferrate film based full device for overall water splitting*, ACS Appl. Mater. Interfaces. **9** (2017) 18015.
[19] R. G. Pearson, *Hard and Soft Acids and Bases*, J. Am. Chem. Soc. **85** (1963) 3533.
[20] J. Wang, T. Qiu, X. Chen, Y. Lu and W. Yang, *Hierarchical hollow urchin-like $NiCo_2O_4$ nanomaterial as electrocatalyst for oxygen evolution reaction in alkaline medium*, J. Power Sources. **268** (2014) 341.
[21] Y. Li, J. Xu, T. Feng, Q. Yao, J. Xie and H. Xia, *Fe_2O_3 Nanoneedles on Ultrafine Nickel Nanotube Arrays as Efficient Anode for High-Performance Asymmetric Supercapacitors*, Adv. Funct. Mater. **27** (2017) 1606728.
[22] F. Wu, X. Guo, G. Hao, Y. Hu and W. Jiang, *Self-supported hollow $Co(OH)_2$/NiCo sulfide hybrid nanotube arrays as efficient electrocatalysts for overall water splitting*, J. Solid State Electrochem. **23** (2019) 2627.
[23] B. Sidhureddy, J. S. Dondapati, A. Chen, *Shape-controlled synthesis of Co_3O_4 for enhanced electrocatalysis of the oxygen evolution reaction*, Chem. Commun. **55** (2019) 3626.
[24] K. Zhang, G. Zhang, J. Qu and H. Liu, *Disordering the Atomic Structure of Co(II) Oxide via B-Doping: An Efficient Oxygen Vacancy Introduction Approach for High Oxygen Evolution Reaction Electrocatalysts*, Small **14** (2018) e1802760.
[25] F. Dionigi, Z. Zeng, I. Sinev, T. Merzdorf, S. Deshpande, M.B. Lopez *et al.*, *In-situ structure and catalytic mechanism of NiFe and CoFe layered double hydroxides during oxygen evolution*, Nat. Commun. **11** (2020) 2522.